HHS Public Access

Author manuscript

Int J Radiat Oncol Biol Phys. Author manuscript; available in PMC 2017 August 01.

Published in final edited form as:

Int J Radiat Oncol Biol Phys. 2016 August 1; 95(5): 1504–1512. doi:10.1016/j.ijrobp.2016.03.018.

Robust Intratumor Partitioning to Identify High-Risk Subregions in Lung Cancer: A Pilot Study

Jia Wu, PhD[1], **Michael F. Gensheimer, MD**[1], **Xinzhe Dong, MD**[1], **Daniel L. Rubin, MD, MS**[2,3], **Sandy Napel, PhD**[2], **Maximilian Diehn, MD, PhD**[1,4,5], **Billy W. Loo Jr., MD, PhD**[1,4], and **Ruijiang Li, PhD**[1,4,*]

[1]Department of Radiation Oncology, Stanford University School of Medicine, Stanford, California

[2]Department of Radiology, Stanford University School of Medicine, Stanford, California

[3]Department of Medicine (Biomedical Informatics Research), Stanford University School of Medicine, Stanford, California

[4]Stanford Cancer Institute, Stanford University School of Medicine, Stanford, California

[5]Institute for Stem Cell Biology and Regenerative Medicine, Stanford University School of Medicine, Stanford, California

Abstract

Purpose—To develop an intra-tumor partitioning framework for identifying high-risk subregions from 18F-fluorodeoxyglucose positron emission tomography (FDG-PET) and CT imaging, and to test whether tumor burden associated with the high-risk subregions is prognostic of outcomes in lung cancer.

Methods and Materials—In this institutional review board-approved retrospective study, we analyzed the pre-treatment FDG-PET and CT scans of 44 lung cancer patients treated with radiotherapy. A novel, intra-tumor partitioning method was developed based on a two-stage clustering process: first at patient-level, each tumor was over-segmented into many superpixels by k-means clustering of integrated PET and CT images; next, tumor subregions were identified by merging previously defined superpixels via population-level hierarchical clustering. The volume associated with each of the subregions was evaluated using Kaplan-Meier analysis regarding its prognostic capability in predicting overall survival (OS) and out-of-field progression (OFP).

Results—Three spatially distinct subregions were identified within each tumor, which were highly robust to uncertainty in PET/CT co-registration. Among these, the volume of the most metabolically active and metabolically heterogeneous solid component of the tumor was predictive of OS and OFP on the entire cohort, with a concordance index or CI = 0.66–0.67. When restricting the analysis to patients with stage III disease (n = 32), the same subregion achieved an even higher CI = 0.75 (HR = 3.93, logrank p = 0.002) for predicting OS, and a CI = 0.76 (HR = 4.84, logrank p = 0.002) for predicting OFP. In comparison, conventional imaging markers including tumor

*CORRESPONDING AUTHOR: Ruijiang Li, PhD, Department of Radiation Oncology, Stanford University School of Medicine, 1070 Arastradero Rd, Palo Alto, CA 94304, rli2@stanford.edu; Tel.: 650-724-5382.

NOTE:

RL, BWL, and MD share senior authorship.

volume, SUV_{max} and MTV_{50} were not predictive of OS or OFP, with CI mostly below 0.60 (logrank $p > 0.05$).

Conclusion—We propose a robust intra-tumor partitioning method to identify clinically relevant, high-risk subregions in lung cancer. We envision that this approach will be applicable to identifying useful imaging biomarkers in many cancer types.

INTRODUCTION

Imaging with FDG-PET and CT plays an important role in the clinical management of non-small cell lung cancer (NSCLC), including diagnosis, staging, radiation treatment planning, and response evaluation (1–3). Recent studies suggested that simple imaging characteristics (4–10), such as tumor size, maximum SUV and metabolic tumor volume, may have prognostic value. However, the prediction accuracy of current prognostic imaging biomarkers in NSCLC is quite limited (4). For example, a recent study (11) reported a concordance index or c-index of 0.62 for predicting overall survival in locally advanced NSCLC based on quantitative imaging features of FDG-PET that include texture features (c-index ranges from 0 to 1; random guess would give 0.5). As accurate prognostication is crucial for tailoring therapy base on individual patient's risk, there is an unmet need to identify reliable biomarkers based on noninvasive imaging characteristics.

A number of studies have focused on extracting advanced, quantitative image features from clinical images to predict lung cancer prognosis (12–17). Given that FDG-PET and CT provide complementary information (metabolic vs anatomic), the image features based on either modality likely represent a partial view of the tumor. Another, perhaps more fundamental limitation of previous approaches is the lack of considering spatial information, where the imaging features were calculated as aggregate measures on the entire tumor volume. Such approaches implicitly assume that the tumor is homogeneous, or heterogeneous but uniformly mixed throughout the whole volume. In reality, however, regional variations within the tumor are often apparent on imaging (18–20). Some parts of the tumor are biologically more aggressive than others and may play a dominant role in disease progression. Failure to explicitly account for these regional variations may obscure the subtle differences among tumors and limit our ability to discover useful imaging biomarkers (18).

There is emerging evidence suggesting that explicitly incorporating spatial information on CT (21), e.g., necrosis in the core and proliferation along the periphery, may lead to improved prediction of survival in NSCLC. However, the simple division into tumor core and boundary regions does not take into account other kinds of spatial variations in tumors that may occur, and the assumption that these regions have different underlying biology may not hold true for all tumors. More sophisticated, potentially more effective image analysis techniques are needed to incorporate tumor-specific regional variations by leveraging the differential information of multi-modality PET/CT imaging.

In this work, we propose a novel approach to developing prognostic imaging signatures for NSCLC. Based on the hypothesis that regional differences within a tumor reflect differing fundamental biological processes, we perform intra-tumor partition through an integrated

analysis of PET and CT images routinely acquired for radiation treatment planning. We show that multiple, spatially distinct subregions exist within tumors and that they can be reliably extracted in a robust fashion across patients. Further, we demonstrate that the volume of one particular subregion predicts overall survival and metastasis, demonstrating superior performance over existing prognostic imaging metrics in lung cancer.

METHODS AND MATERIALS

Patient population

Under approval from the institutional review board, we retrospectively reviewed records and images of 44 lung cancer patients, who were treated with definitive radiotherapy or concurrent chemoradiotherapy at our institution from October 2005 through December 2009. A majority of the patients (n=32) had stage III disease, and others had stage I, II, or IV disease. In our institution, we follow all NSCLC patients at regular intervals (usually every 3 months) after treatment. During the follow-up, 32 patients (72.7%) died and 23 patients (52.3%) had an out-of-field failure. Patient characteristics are summarized in Table 1.

PET/CT imaging

All patients underwent PET/CT imaging for radiation treatment planning prior to radiotherapy. Regarding the imaging protocol, following an 8 h fast, patients were injected with 10–18 mCi of FDG, with imaging 60 min later on a GE Discovery PET/CT scanner (GE Medical Systems, Milwaukee, WI). CT images were collected in the helical acquisition mode. In the same scan locations and generally spanning around seven-bed positions, PET data were acquired in 2D mode, with 3 to 5 min of acquisition time per bed position. The PET images were then reconstructed with an ordered set expectation maximization algorithm, with the CT data for attenuation correction. A separate non-contrast enhanced CT scan was performed at the end of the natural exhale. The complete PET/CT examination requires approximately one and a half hours, including patient setup, tracer uptake, and image acquisition. The spatial resolution of the original PET image was $2.34 \times 2.34 \times 3.27$ mm^3 and the spatial resolution of the original CT image was $0.98 \times 0.98 \times 1.25$ mm^3.

Intra-tumor partitioning by integrated analysis of PET/CT imaging

Here, we propose a multi-parametric intra-tumor partitioning method to consistently divide the entire tumor into multiple spatially distinct subregions. Figure 1 summarizes the complete pipeline that contains three key steps. The first step is to accurately align the PET and CT images for each patient. The second step aims to independently segment the entire tumor into a large number of superpixels, where neighboring voxels with similar imaging characteristics are grouped together. Finally, similar superpixels within the same tumor are merged to form larger, dominant subregions via population-level clustering. This process also establishes the correspondence of the subregions so that they can be compared across patients.

In more details, PET and CT images of the same patient were first rigidly registered using the elastix software (22). The primary tumor was contoured on the CT image by an experienced radiation oncologist as part of the radiation treatment planning. In addition to

the original voxel intensity on CT and PET, the local entropy (9-by-9-by-9 neighborhood) of CT and PET, which measures intra-tumor heterogeneity locally, was also computed at each voxel and incorporated into the analysis, leading to a four-dimensional feature vector. For patient-level tumor over-segmentation, the k-means clustering algorithm with spatial constraint (23) was used to group voxels with similar features together for each tumor, with squared Euclidean distance as the distance measure.

In the population-level clustering step, each superpixel was characterized by the mean feature vector (the four aforementioned signals). Gathering the superpixels of all patients together, hierarchical clustering (24) was applied to explore both inter- and intra-patient similarity, using the average linkage and Euclidean distance. Both dendrogram and heat map were used to show the clustering results as well as to resolve the population-level labeling output (i.e., the number of clusters and their hierarchical relationships). The number of clusters was determined using the gap statistic (25). Consequently, the entire tumor was consistently partitioned into several subregions, and each demonstrates distinct PET and CT imaging characteristics. The k-means and hierarchical clustering were implemented with MATLAB (MathWorks, Natick, Massachusetts).

Sensitivity of intra-tumor partition with respect to PET/CT registration

While modern PET/CT scanners acquire both PET and CT that are co-registered, the CT component is used for attenuation correction purposes and its image quality is suboptimal with large slice thickness and lower mAs. Here, we are using the high-quality CT used for radiation treatment planning, which is not automatically registered with the PET. Moreover, in lung cancer, tumor motion between scans usually brings about additional uncertainty that would require a careful co-registration between PET and CT. We investigated the sensitivity of the intra-tumor partition results given the uncertainty of registration between PET and CT. We simulated the registration uncertainty by intentionally shifting the original CT image away from the PET image for 3 mm (26) along a randomly picked direction among all six directions in 3D. Then, we quantitatively assessed the consistency between the clustering results with and without the random shift. The in-group proportion (IGP) (27) was selected to test the reproducibility of the clustering results. In brief, the IGP indicates whether one cluster in one dataset is similar to another cluster in another dataset. When IGP is 100%, the clusters from two datasets are identical. More importantly, the robustness of the main prognostic factors tested in this study, i.e., the volumes associated with distinct tumor subregions, were evaluated against registration uncertainty.

Prognostic evaluation and statistical analysis

The tumor volume associated with each dominant subregion was identified as a putative biomarker of treatment outcomes for further validation. The Cox proportional hazard model was used to evaluate each imaging feature in terms of their prognostic capability for both overall survival (OS) and freedom from out-of-field progression (OFP). We used the median value of the predicted hazard/risk to divide the cohort into high- versus low-risk groups. Concordance index (CI) was used to assess the prognostic capability of the imaging biomarkers. Kaplan-Meier analysis was used to estimate the probability of a certain event. The statistical significance of CIs and whether one CI was higher than another were assessed

via bootstrapping. In details, for testing the statistical significance of the CI, the original survival data was firstly permutated. Then both the original and permutated survival data were bootstrapped to a sample size 50 with 100 replications. Lastly, the CI distributions from both bootstrapped samples were compared via the Wilcoxon signed rank test. A p-value < 0.05 is considered as statistically significant. The Cox survival modeling and statistical analysis were performed in R.

RESULTS

Three dominant intra-tumor subregions emerged

The intra-tumor partitioning method identified three major clusters or tumor subregions that show distinct imaging phenotypes (Figure 2, Supplementary Figures 1 and 2). Here, three clusters showed the optimal gap metric among 2 to 10 clusters. The first cluster, labeled as cluster A, was associated with high PET SUV, high CT number and high PET entropy. This particular region contains the most metabolically active and heterogeneous solid tumor component. The second cluster, labeled as cluster B, was associated with low PET SUV, low PET entropy and high CT number, which contains the metabolically non-active solid component of the tumor. The third cluster, labeled as cluster C, contains low CT number regions, i.e., non-solid component. Two outliers with a negligibly small volume (labeled as cluster E1 and E2) were excluded for further analysis.

Intra-tumor partitioning was robust against PET/CT misalignment

For patient-level over-segmentation, the median of IGP was 95.5% with a range from 80.0% to 100%, which indicates highly similar clusters between the k-means clustering results with and without random shift of 3 mm. For population-level labeling, there were still three dominant sub-regions (refer to the Supplementary Figure 3 for the corresponding dendrogram and heat map), and the IGP for these three main clusters were 98.3%, 98.2% and 98.6%. More importantly, Supplementary Figure 4 showed a very strong linear correlation ($R^2 > 0.95$, $p < 0.001$) of the derived tumor volume of all three tumor clusters with and without shift. Together, these data show that the proposed framework was able to identify robust intra-tumor regions despite uncertainty in PET/CT registration.

The volume of high-risk subregion was predictive of outcomes

In the entire cohort (n=44), the tumor volume associated with cluster A was prognostic of OS, with a CI = 0.67 (p = 2.67e-32) and hazard ratio or HR = 2.79 (logrank p = 0.004) for separating low- vs high-risk patients, as shown in Figure 3a. In terms of predicting OFP, the same subregion achieved a good CI = 0.66 (p = 3.78e-26), with HR = 2.07 (logrank p = 0.08), as shown in Figure 3b. These results compared favorably (p<0.001) with conventional imaging metrics, where total tumor volume, SUV_{max} and MTV_{50} were not prognostic of OS or OFP (see Supplementary Figures 5, 6 and 7).

When restricting our analysis to stage III patients (n=32), the prognostic capability of the high-risk tumor volume was further improved. For predicting OS it achieved a CI = 0.75 (p = 2.33e-34) and HR = 3.93 (logrank p = 0.002) as shown in Figure 3c, and for predicting OFP it achieved a CI = 0.76 (p = 2.88e-34) and HR = 4.84 (logrank p = 0.002) as shown in

Figure 3d. Again, these results significantly ($p<0.001$) improved the prognostic capability compared with conventional imaging metrics (see Supplementary Figures 5, 6 and 7).

Figure 4 shows the process of using the proposed method to analyze two representative patients. Both patients had stage IIIb lung cancer, with similar tumor volume but very different outcomes: patient 1 was still alive and free from out-of-field progression during a 4-year follow-up, while patient 2 deceased after three months. SUV_{max} and MTV_{50} of patient 1 were higher than patient 2, contrary to prior studies indicating that higher SUV and MTV correlate with poor survival. On the other hand, using our proposed method, patient 1 actually had a smaller volume of high-risk subregion (i.e., cluster A) than patient 2, consistent with the clinical outcomes.

Multivariate analysis

To evaluate whether the proposed imaging biomarker provided independent prognostic information, we performed multivariate analyses to predict OS for the entire cohort as well as for the stage III cohort. Both the high-risk tumor volume and the gross tumor volume were included, which were further adjusted for clinical factors, i.e., Karnofsky Performance Status (KPS), radiotherapy dose, stage, concurrent chemotherapy status, age, and gender. After adjustment, the volume of high-risk subregion remained statistically significant as an independent predictor of OS for both the entire cohort ($p = 0.03$) and the stage III patient cohort ($p = 0.001$), as shown in Table 2. In comparison, gross tumor volume was not an independent predictor of OS in either cohort based on multivariate analysis. Since the high-risk tumor volume was the only prognostic predictor for OFP, we did not perform a multivariate analysis for that.

DISCUSSION

In this study, we proposed a two-stage multi-parametric clustering approach to identify clinically relevant, high-risk subregions through an integrated analysis of PET/CT images in lung cancer. We found three intra-tumor subregions with distinct imaging features, and their volumes were robust against uncertainty in registration between PET and CT. In addition, they were robust to the initial number of over-segmented tumor regions (both 20 and 10 led to almost identical results), largely due to their merging during the population-level clustering. The tumor volume associated with the most metabolically active and metabolically heterogeneous solid component was prognostic of overall survival and metastasis, which consistently outperformed three conventional imaging metrics. Biologically, the high-risk subregion we identified may represent the most proliferative and hypoxic portions of the tumor (28, 29), explaining its prognostic value.

Intra-tumor heterogeneity is reflected on multiple spatial scales (at molecular, cellular, and tissue level) and has been associated with aggressive disease and poor prognosis (30–34). While regional differences are often observed on imaging and are an important manifestation of intra-tumor heterogeneity, their clinical significance has not been systematically investigated. It is plausible that some parts of the tumor are more aggressive than others, and the tumor volume associated with these high-risk regions could determine disease progression and ultimately patient survival, and thus may be more reliable

biomarkers of clinical outcomes. In this work, we have used local entropy as a simple measurement of phenotypic complexity of the tumor. In principle, more texture features that capture additional aspects of tumor heterogeneity could be incorporated into the proposed framework.

This study is among the first to explicitly extract subregions from heterogonous tumors and explore their clinical significance in disease prognosis (21, 35). Besides the obvious differences in disease sites (NSCLC versus GBM and head-and-neck cancer) and imaging modalities (FDG-PET/CT versus MRI), The proposed method differs from prior studies in several key aspects: 1) our method is based on a two-stage clustering process, where the first patient-level over-segmentation generates superpixels that are robust to image noise, and the second population-level clustering produces consistently defined subregions across the entire cohort, while prior methods were based on direct single-stage clustering; 2) our method does not assume a predefined number of intra-tumor clusters but rather learns this number from all available data; 3) instead of only considering voxel values, we incorporate both magnitude of image signal and its spatial heterogeneity map (measured with local entropy) in defining the intra-tumor clusters. Another recent study (36) proposed a three-class fuzzy locally adaptive Bayesian (3-FLAB) for the delineation of inhomogeneous tumors. However, the method was based on a single image modality (FDG-PET), limited to a fixed number of (i.e., 2) intra-tumor subregions. The clinical significance (e.g., prognostic value) of either subregion defined as such was unclear from the study (36).

Biomarkers that can reliably predict treatment failure on an individualized basis will have tremendous value in guiding the optimal treatment of lung cancer. The need for predictive biomarkers is highlighted by a recent randomized phase 3 trial (Radiation therapy oncology group or RTOG 0617) that failed to show a survival benefit of high-dose versus standard-dose radiotherapy in locally advanced NSCLC (37). Instead of delivering intensive therapy to an unselected population, reliable biomarkers could be used to identify those patients at highest risk of distant progression who may benefit from additional systemic therapy.

Our study has several limitations. This is a retrospective study with a relatively small cohort. To apply the integrated analysis, accurate co-registration between PET and CT is required, although we showed that the volume of high-risk subregion was robust against this kind of uncertainty of a reasonable amount (3 mm). Another technical limitation is 3D PET acquisition in the presence of respiratory motion, which could lead to distortion of the true metabolic activity, especially for tumors located close to the diaphragm. Respiratory-gated and 4D PET acquisition (38) may help improve the quantitative accuracy of PET imaging.

Finally, the prognostic value of the new imaging biomarker needs to be evaluated on large prospective cohorts in future studies. The volume of the high-risk subregion prior to treatment did not predict local failure (or in-field progression) in our study population. It would be interesting to include longitudinal scans (39, 40) during follow up and investigate whether the changes in the imaging feature could be useful in predicting local failure.

CONCLUSION

We have developed a robust, intra-tumor partitioning framework to identify clinically relevant subregions within a tumor by integrating FDG-PET and CT images. The volume of a high-risk subregion characterized by the most metabolically active and metabolically heterogeneous solid component of the tumor is predictive of survival and out-of-field progression in NSCLC. Its prognostic value needs to be confirmed in prospective large cohorts.

Supplementary Material

Refer to Web version on PubMed Central for supplementary material.

Acknowledgments

This work was partially supported by NIH grants R00 CA166186, R01 CA160251, U01 CA190214.

References

1. Fischer B, Lassen U, Mortensen J, et al. Preoperative staging of lung cancer with combined PET-CT. The New England journal of medicine. 2009; 361(1):32–9. [PubMed: 19571281]
2. Ciernik IF, Dizendorf E, Baumert BG, et al. Radiation treatment planning with an integrated positron emission and computer tomography (PET/CT): a feasibility study. International journal of radiation oncology, biology, physics. 2003; 57(3):853–63.
3. Ohri N, Duan F, Machtay M, et al. Pretreatment FDG-PET Metrics in Stage III Non-Small Cell Lung Cancer: ACRIN 6668/RTOG 0235. Jnci-J Natl Cancer I. 2015; 107(4)
4. Machtay M, Duan F, Siegel BA, et al. Prediction of survival by [18F]fluorodeoxyglucose positron emission tomography in patients with locally advanced non-small-cell lung cancer undergoing definitive chemoradiation therapy: results of the ACRIN 6668/RTOG 0235 trial. J Clin Oncol. 2013; 31(30):3823–30. [PubMed: 24043740]
5. Nair VJ, MacRae R, Sirisegaram A, Pantarotto JR. Pretreatment [F-18]-fluoro-2-deoxy-glucose Positron Emission Tomography Maximum Standardized Uptake Value as Predictor of Distant Metastasis in Early-Stage Non-Small Cell Lung Cancer Treated With Definitive Radiation Therapy: Rethinking the Role of Positron Emission Tomography in Personalizing Treatment Based on Risk Status. Int J Radiat Oncol. 2014; 88(2):312–8.
6. Satoh Y, Onishi H, Nambu A, Araki T. Volume-based Parameters Measured by Using FDG PET/CT in Patients with Stage I NSCLC Treated with Stereotactic Body Radiation Therapy: Prognostic Value. Radiology. 2014; 270(1):275–81. [PubMed: 24029640]
7. Lee P, Bazan JG, Lavori PW, et al. Metabolic Tumor Volume is an Independent Prognostic Factor in Patients Treated Definitively for Non-Small-Cell Lung Cancer. Clin Lung Cancer. 2012; 13(1):52–8. [PubMed: 21703935]
8. Liao S, Penney BC, Wroblewski K, et al. Prognostic value of metabolic tumor burden on 18F-FDG PET in nonsurgical patients with non-small cell lung cancer. European journal of nuclear medicine and molecular imaging. 2012; 39(1):27–38. [PubMed: 21946983]
9. Guerra JLL, Gladish G, Komaki R, Gomez D, Zhuang Y, Liao ZX. Large Decreases in Standardized Uptake Values After Definitive Radiation Are Associated with Better Survival of Patients with Locally Advanced Non-Small Cell Lung Cancer. J Nucl Med. 2012; 53(2):225–33. [PubMed: 22241911]
10. van Elmpt W, Ollers M, Dingemans AMC, Lambin P, De Ruysscher D. Response Assessment Using F-18-FDG PET Early in the Course of Radiotherapy Correlates with Survival in Advanced-Stage Non-Small Cell Lung Cancer. J Nucl Med. 2012; 53(10):1514–20. [PubMed: 22879081]

11. Fried DV, Mawlawi O, Zhang L, et al. Stage III Non–Small Cell Lung Cancer: Prognostic Value of FDG PET Quantitative Imaging Features Combined with Clinical Prognostic Factors. Radiology. 2016; 278(1):214–22. [PubMed: 26176655]
12. Coroller TP, Grossmann P, Hou Y, et al. CT-based radiomic signature predicts distant metastasis in lung adenocarcinoma. Radiotherapy and oncology: journal of the European Society for Therapeutic Radiology and Oncology. 2015; 114(3):345–50. [PubMed: 25746350]
13. Aerts HJ, Velazquez ER, Leijenaar RT, et al. Decoding tumour phenotype by noninvasive imaging using a quantitative radiomics approach. Nat Commun. 2014; 5:4006. [PubMed: 24892406]
14. Hatt M, Majdoub M, Vallieres M, et al. F-18-FDG PET Uptake Characterization Through Texture Analysis: Investigating the Complementary Nature of Heterogeneity and Functional Tumor Volume in a Multi-Cancer Site Patient Cohort. J Nucl Med. 2015; 56(1):38–44. [PubMed: 25500829]
15. Fried DV, Tucker SL, Zhou S, et al. Prognostic value and reproducibility of pretreatment CT texture features in stage III non-small cell lung cancer. International Journal of Radiation Oncology* Biology* Physics. 2014; 90(4):834–42.
16. Vallieres M, Freeman CR, Skamene SR, El Naqa I. A radiomics model from joint FDG-PET and MRI texture features for the prediction of lung metastases in soft-tissue sarcomas of the extremities. Physics in medicine and biology. 2015; 60(14):5471–96. [PubMed: 26119045]
17. XXX. (Blinded for review).
18. Gatenby RA, Grove O, Gillies RJ. Quantitative imaging in cancer evolution and ecology. Radiology. 2013; 269(1):8–15. [PubMed: 24062559]
19. O'Connor JPB, Rose CJ, Waterton JC, Carano RAD, Parker GJM, Jackson A. Imaging Intratumor Heterogeneity: Role in Therapy Response, Resistance, and Clinical Outcome. Clin Cancer Res. 2015; 21(2):249–57. [PubMed: 25421725]
20. Farjam R, Tsien CI, Feng FLY, et al. Physiological Imaging-Defined, Response-Driven Subvolumes of a Tumor. Int J Radiat Oncol. 2013; 85(5):1383–90.
21. Grove O, Berglund AE, Schabath MB, et al. Quantitative Computed Tomographic Descriptors Associate Tumor Shape Complexity and Intratumor Heterogeneity with Prognosis in Lung Adenocarcinoma. Plos One. 2015; 10(3)
22. Klein S, Staring M, Murphy K, Viergever MA, Pluim JP. elastix: a toolbox for intensity-based medical image registration. IEEE transactions on medical imaging. 2010; 29(1):196–205. [PubMed: 19923044]
23. Kanungo T, Mount DM, Netanyahu NS, Piatko CD, Silverman R, Wu AY. An efficient k-means clustering algorithm: Analysis and implementation. Ieee T Pattern Anal. 2002; 24(7):881–92.
24. Johnson SC. Hierarchical Clustering Schemes. Psychometrika. 1967; 32(3):241–54. [PubMed: 5234703]
25. Tibshirani R, Walther G, Hastie T. Estimating the number of clusters in a data set via the gap statistic. Journal of the Royal Statistical Society: Series B (Statistical Methodology). 2001; 63(2): 411–23.
26. Fortin D, Basran PS, Berrang T, Peterson D, Wai ES. Deformable versus rigid registration of PET/CT images for radiation treatment planning of head and neck and lung cancer patients: a retrospective dosimetric comparison. Radiat Oncol. 2014; 9(1):50. [PubMed: 24512755]
27. Kapp AV, Tibshirani R. Are clusters found in one dataset present in another dataset? Biostatistics. 2007; 8(1):9–31. [PubMed: 16613834]
28. Vesselle H, Schmidt RA, Pugsley JM, et al. Lung cancer proliferation correlates with [F-18] fluorodeoxyglucose uptake by positron emission tomography. Clin Cancer Res. 2000; 6(10):3837–44. [PubMed: 11051227]
29. Zegers CM, van Elmpt W, Reymen B, et al. In vivo quantification of hypoxic and metabolic status of NSCLC tumors using [18F] HX4 and [18F] FDG-PET/CT imaging. Clin Cancer Res. 2014; 20(24):6389–97. [PubMed: 25316821]
30. Win T, Miles KA, Janes SM, et al. Tumor Heterogeneity and Permeability as Measured on the CT Component of PET/CT Predict Survival in Patients with Non-Small Cell Lung Cancer. Clin Cancer Res. 2013; 19(13):3591–9. [PubMed: 23659970]

31. Cook GJ, O'Brien ME, Siddique M, et al. Non-Small Cell Lung Cancer Treated with Erlotinib: Heterogeneity of F-FDG Uptake at PET-Association with Treatment Response and Prognosis. Radiology. 2015:141309.
32. Cook GJ, Yip C, Siddique M, et al. Are pretreatment 18F-FDG PET tumor textural features in non-small cell lung cancer associated with response and survival after chemoradiotherapy? J Nucl Med. 2013; 54(1):19–26. [PubMed: 23204495]
33. Cui Y, Tha KK, Terasaka S, et al. Prognostic Imaging Biomarkers in Glioblastoma: Development and Independent Validation on the Basis of Multiregion and Quantitative Analysis of MR Images. Radiology. 2015:150358.
34. El Naqa I, Grigsby P, Apte A, et al. Exploring feature-based approaches in PET images for predicting cancer treatment outcomes. Pattern recognition. 2009; 42(6):1162–71. [PubMed: 20161266]
35. Wang P, Popovtzer A, Eisbruch A, Cao Y. An approach to identify, from DCE MRI, significant subvolumes of tumors related to outcomes in advanced head-and-neck cancer. Medical physics. 2012; 39(8):5277–85. [PubMed: 22894453]
36. Hatt M, Le Rest CC, Descourt P, et al. Accurate automatic delineation of heterogeneous functional volumes in positron emission tomography for oncology applications. International Journal of Radiation Oncology* Biology* Physics. 2010; 77(1):301–8.
37. Bradley JD, Paulus R, Komaki R, et al. Standard-dose versus high-dose conformal radiotherapy with concurrent and consolidation carboplatin plus paclitaxel with or without cetuximab for patients with stage IIIA or IIIB non-small-cell lung cancer (RTOG 0617): a randomised, two-by-two factorial phase 3 study. The Lancet Oncology. 2015; 16(2):187–99. [PubMed: 25601342]
38. Nehmeh S, Erdi Y, Pan T, et al. Four-dimensional (4D) PET/CT imaging of the thorax. Medical physics. 2004; 31(12):3179–86. [PubMed: 15651600]
39. Toma-Dasu I, Uhrdin J, Lazzeroni M, et al. Evaluating Tumor Response of Non-Small Cell Lung Cancer Patients With 18 F-Fludeoxyglucose Positron Emission Tomography: Potential for Treatment Individualization. International Journal of Radiation Oncology* Biology* Physics. 2015; 91(2):376–84.
40. Zhang H, Tan S, Chen W, et al. Modeling pathologic response of esophageal cancer to chemoradiation therapy using spatial-temporal 18 F-FDG PET features, clinical parameters, and demographics. International Journal of Radiation Oncology* Biology* Physics. 2014; 88(1):195–203.

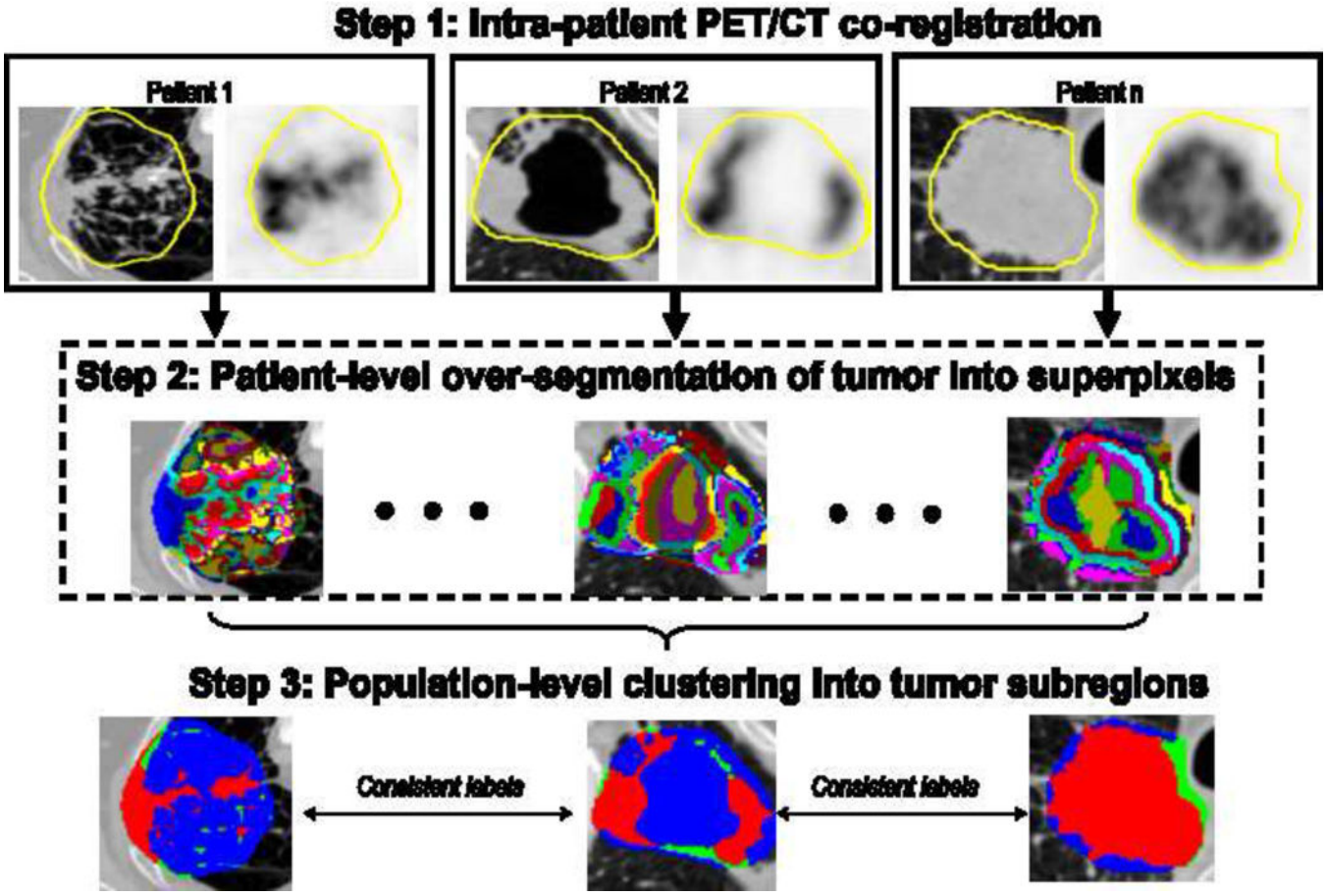

Figure 1.
Overall flowchart of the proposed intra-tumor partitioning method.

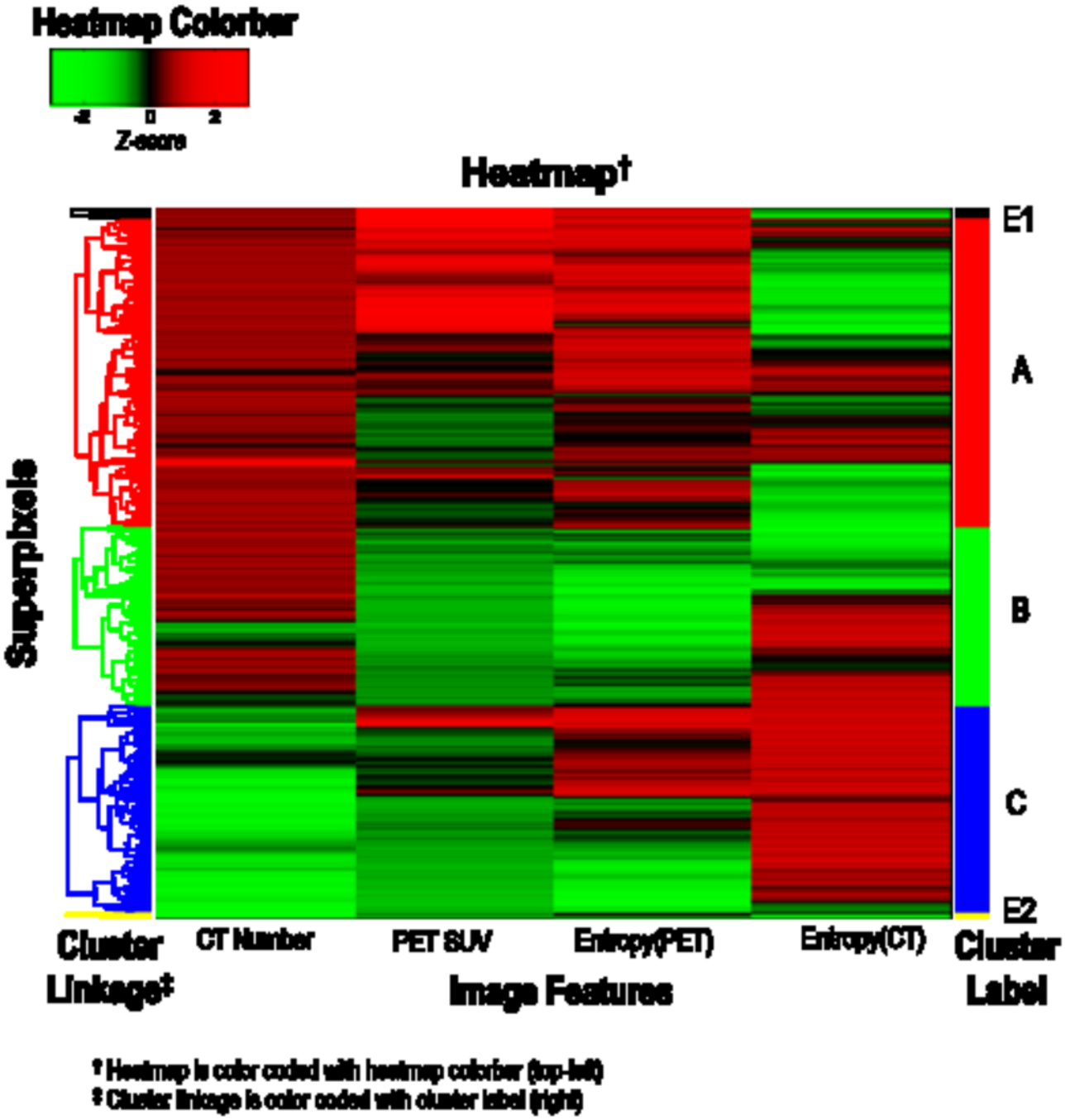

Figure 2.

Identification of intra-tumor subregions based on population-level hierarchical clustering of the over-segmented superpixels (20 per patients) for the entire cohort (n=44).

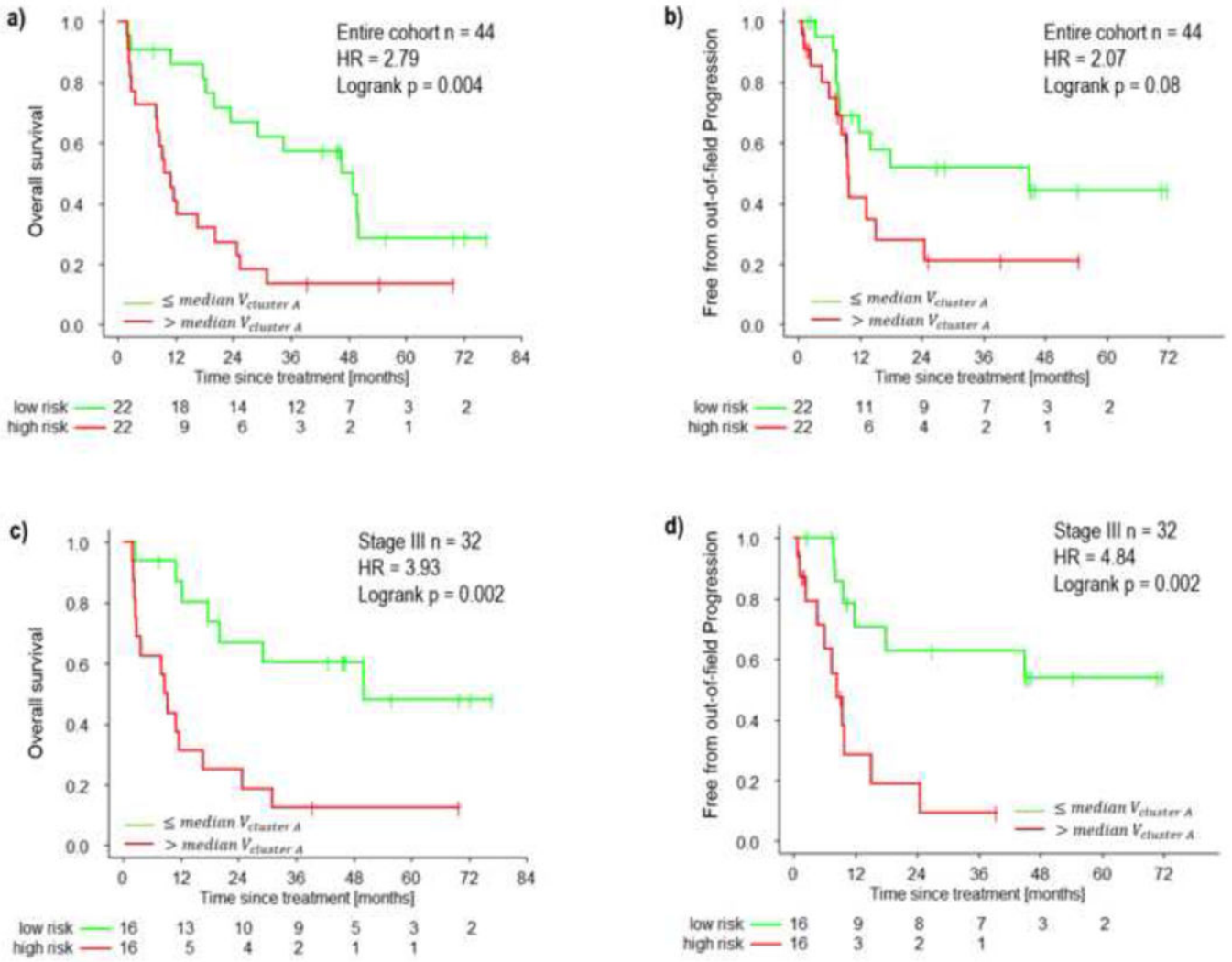

Figure 3.

Kaplan-Meier curves of using tumor volume of the high-risk subregion (i.e., cluster A) to predict: a) overall survival, b) out-of-field progression, for the entire cohort (n = 44), and c) overall survival, d) out-of-field progression, for patients with stage III disease (n = 32). The cutoff between high vs low-risk patients was determined based on the median of predicted risk.

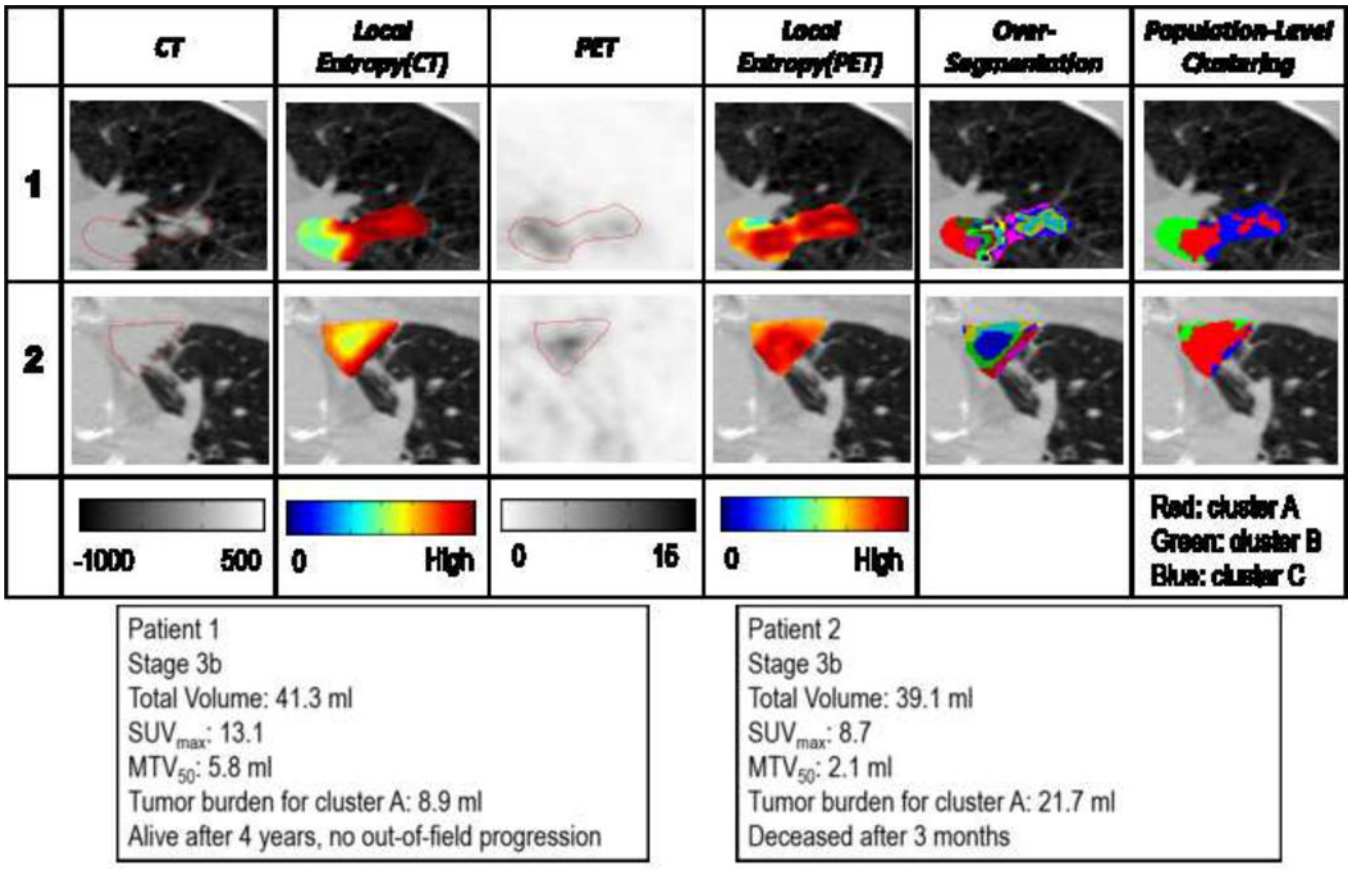

Figure 4.
Details of implementing the proposed tumor partitioning method to analyze two representative patients.

Table 1

Demographic Data for the Study Cohort

	N = 44
Age: median (range)	69.5(47.2–89.7)
Gender: M/F	24(54.5%)/20(45.5%)
Stage: (1a/1b/2a/2b/3a/3b/4)	4(9.0%)/3(6.8%)/1(2.3%)/1(2.3%)/12(27.3%)/20(45.5%)/3(6.8%)
Concurrent Chemotherapy: Y/N	34(77.3%)/10(22.7%)
Radiotherapy dose (Gy): median (range)	68(40–74)
Karnofsky Performance Status	80(50–90)
Follow-up time (month): median (range)	20.2(1.8–76.7)
Death: Y/N	32(72.7%)/12(27.3%)
Out of field Failure: Y/N	23(52.3%)/21(47.7%)

Table 2

Univariate and Multivariate Analysis of the Volume of High-Risk Tumor Subregion (Volume of Cluster A), Gross Tumor Volume and Clinical Factors for Predicting OS of All Patients (N = 44) and Stage III Patients (N = 32).

All Patients (N = 44)						
Predictors for OS	**Univariate**			**Multivariate**		
	HR	**95% CI**	**P-Value**	**HR**	**95% CI**	**P-Value**
High-Risk Tumor Volume	2.79	1.36–5.75	0.004**	1.08	1.01–1.14	0.030*
Gross Tumor Volume	1.73	0.86–3.48	0.123	1.00	0.99–1.01	0.442
Gender	1.02	0.51–2.05	0.948	–	–	–
Age	1.37	0.68–2.75	0.380	–	–	–
Stage (I+II/III+IV)	1.52	0.70–3.34	0.288	–	–	–
Concurrent Chemotherapy	1.37	0.63–2.99	0.424	–	–	–
Radiotherapy Dose	1.17	0.59–2.35	0.653	–	–	–
KPS	2.95	1.45–5.99	0.002**	0.94	0.90–0.99	0.009**
Stage III Patients (N = 32)						
Predictors for OS	**Univariate**			**Multivariate**		
	HR	95% CI	P-Value	HR	95% CI	P-Value
High-Risk Tumor Volume	3.94	1.56–9.92	0.002**	1.2	1.15–1.23	0.001**
Gross Tumor Volume	2.75	1.13–6.72	0.020*	1.00	0.99–1.00	0.410
Gender	1.09	0.46–2.59	0.849	–	–	–
Age	0.78	0.33–1.85	0.570	–	–	–
Stage (3a/3b)	2.10	0.81–5.43	0.118	6.39	1.18–34.82	0.032*
Concurrent Chemotherapy	1.64	0.48–5.60	0.429	–	–	–
Radiotherapy Dose	1.21	0.51–2.86	0.657	–	–	–
KPS	3.77	1.50–9.48	0.003**	0.90	0.83–0.97	0.008**

Note: 1.

* indicates p-value < 0.05;

** indicates p-value <0.01; 2. Non-significant clinical factors were not presented for multivariate analysis. HR: hazard ratio.